

Effect of Polyethylene Glycol, Alkyl, and Oligonucleotide Spacers on the Binding, Secondary Structure, and Self-Assembly of Fractalkine Binding FKN-S2 Aptamer-Amphiphiles

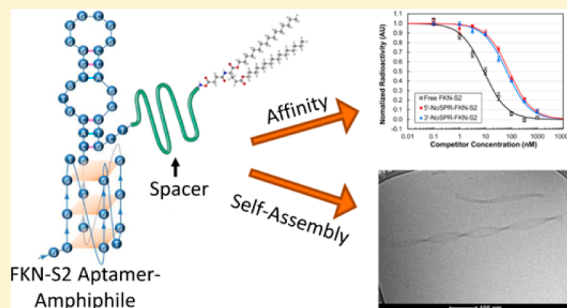
Brett Waybrant,[†] Timothy R. Pearce,[‡] and Efrosini Kokkoli*,[†]

[†]Department of Chemical Engineering and Materials Science, and [‡]Department of Biomedical Engineering, University of Minnesota, Minneapolis, Minnesota 55455, United States

S Supporting Information

ABSTRACT: Previously we identified an aptamer, named FKN-S2, which binds the cell surface protein fractalkine with high affinity and specificity. In this paper a hydrophobic dialkyl C₁₆ tail was added to the aptamer to create an aptamer-amphiphile. We investigated how the tail and a spacer molecule of varying length and hydrophobicity, inserted between the tail and the aptamer headgroup, affect the binding, structure, and self-assembly properties of the aptamer-amphiphile. We synthesized aptamer-amphiphiles with no spacer (NoSPR), polyethylene glycol (PEG₄, PEG₈, PEG₂₄), alkyl (C₁₂ and C₂₄), or oligonucleotide (T₁₀ and T₅; 10 and 5 thymine, and A₁₀; 10 adenine) spacers. The addition of the tail reduced the binding affinity of the aptamer-amphiphile over 7.5-fold compared to the free aptamer.

The hydrophobic alkyl spacers resulted in the greatest loss of affinity, and the hydrophilic PEG spacers improved amphiphile affinity but did not restore it to that of the free aptamer. Interestingly, oligonucleotide spacers produced the highest affinity amphiphiles. Nucleotide composition did not affect affinity, however, as the T₁₀ and A₁₀ spacers had equal affinity. The oligonucleotide spacer amphiphiles had the highest affinity because the oligonucleotide spacer increased the affinity of free aptamer; the FKN-S2 aptamer plus the oligonucleotide spacer had a higher affinity than the free FKN-S2 aptamer. Circular dichroism (CD) spectroscopy and thermal melting studies indicated the aptamer forms a stem-loop and intramolecular G-quadruplex, and the tail strongly stabilized the formation of the G-quadruplex in a buffer. Cryogenic transmission electron microscopy (cryo-TEM) imaging showed the aptamer-amphiphiles, independent of the spacer used, self-assembled into micelles and nanotapes, flat bilayer structures that were often twisted. Finally, liposomes functionalized with the FKN-S2 amphiphile were incubated with fractalkine expressing cells, and the amount of binding was dependent on the concentration of the amphiphile on the liposome surface.



INTRODUCTION

The ability of antibodies to selectively bind a molecular target sparked a revolution in biotechnology leading to the creation of novel diagnostics, therapeutics, and imaging techniques.¹ Aptamers are short strands of nucleic acids that, like antibodies, bind molecular targets with high affinity and specificity. Positive characteristics of aptamers include *in vitro* selection, chemical synthesis, reproducible and specific chemical modifications, and good chemical and thermal stability.^{2,3} Because of these advantages, aptamers are used for sensors and diagnostics,^{4,5} affinity separations,⁶ and drug delivery and imaging applications.^{7,8}

Aptamers are often modified to reduce nuclease digestion,⁹ increase circulation lifetime,¹⁰ increase association with cellular membranes,¹¹ induce micelle formation,¹² or functionalize liposomes.¹³ Commonly a polyethylene glycol (PEG) or an oligo-T (thymine) spacer is added to the aptamer, especially when attaching the aptamer to a surface.¹⁴ However, these modifications can affect the affinity of the aptamer for the target

molecule through steric repulsion or alteration of the aptamer secondary structure.

Amphiphiles often form supramolecular structures.¹⁵ Previous studies have shown that aptamer-amphiphiles can form micelles, which can be used for drug delivery or bottom up assembly.^{16,17} Nucleic acid amphiphiles with a single nucleoside as the headgroup and a 12 carbon dialkyl tail self-assembled into cylindrical micelles and helical ribbons.¹⁸ However, the single nucleoside headgroup lacked ligand–receptor binding capabilities. Recent work by our group has shown that aptamer-amphiphiles with a 25 nucleic acid aptamer headgroup (that binds to Muc-1 glycoprotein) and C₁₆ dialkyl tails (similar to the ones used in this study) self-assembled into micelles when the amphiphile did not contain a spacer (NoSPR) or when a hydrophilic PEG₄ or PEG₈ spacers were used, but self-assembled into micelles and nanotapes, flat or twisted, when

Received: January 29, 2014

Revised: May 19, 2014

Published: May 21, 2014

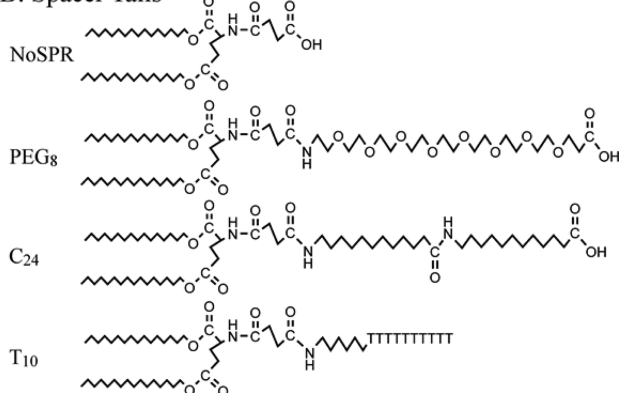
the hydrophobic C₁₂ or C₂₄ spacers were used.¹⁹ The nanotapes, the presence of which could not be predicted by the standard packing parameter analysis, were bilayer structures with the hydrocarbon tails and spacers forming the hydrophobic core and the aptamer headgroups extending away from the hydrophobic interfaces.¹⁹ We hypothesized that the hydrophobic tails and polycarbon spacers, through attractive hydrophobic interactions, forced the aptamer headgroups together, reducing the interfacial headgroup area and thereby allowing nanotape formation.

Previously, we developed the FKN-S2 aptamer that binds to the cell surface protein fractalkine (CX3CL1) with a dissociation constant (K_d) of 3.4 ± 0.7 nM.²⁰ Fractalkine is a chemokine involved in inflammation pathways through the recruitment and adhesion of leukocytes^{21,22} and is expressed on inflamed endothelial cells and certain cancers.²³⁻²⁵ In this work we investigated the effects of the tail and spacer on the affinity, secondary structure, and self-assembly of FKN-S2 amphiphiles. The 40-mer FKN-S2 aptamer (sequence shown in Figure 1A)

A: FKN-S2 Sequence



B: Spacer Tails



C: Amphiphile Structure

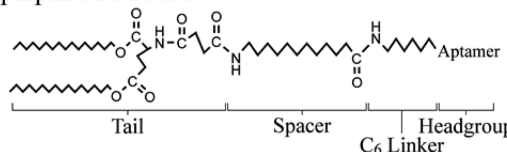


Figure 1. (A) The sequence of the FKN-S2 aptamer with the 3' C₆ linker, (B) structures of the tail, a saturated dialkyl C₁₆ lipid like molecule, with a subset of the different spacers: NoSPR (no spacer was used), PEG₃, C₂₄, and T₁₀, and (C) structure of the aptamer-amphiphile with a C₁₂ spacer. The aptamer was purchased with a six carbon amino linker (C₆ linker) on either the 5' or 3' end to which the tail was conjugated.

was synthesized with a six carbon (C_6) amino linker added to either the 5' or 3' end of the aptamer. Tails with different spacers (a subset of which are shown in Figure 1B) were then conjugated to the C_6 linker creating the aptamer-amphiphile (Figure 1C). The effect of the tail and different spacers on the aptamer-amphiphile binding affinity for fractalkine was measured using a competition binding assay. The aptamer and aptamer-amphiphile secondary structure were probed with circular dichroism (CD) spectroscopy and thermal melting analysis to investigate the effect of the tail on secondary

structure. Cryogenic transmission electron microscopy (cryo-TEM) was used to visualize the self-assembled structures of the FKN-S2 aptamer-amphiphiles and a 40-mer oligonucleotide with a similar secondary structure. Finally, considering that the FKN-S2 aptamer can be used to functionalize nanoparticles, liposomes were functionalized with a FKN-S2 amphiphile and targeted to fractalkine expressing cells as a targeted drug delivery proof of concept.

EXPERIMENTAL SECTION

Full experimental details can be found in the Supporting Information.

Synthesis of Aptamer-Amphiphiles. The tails were synthesized by conjugating two cetyl alcohols to the carboxyl groups of L-glutamic acid and adding a succinic acid linker to the amino group.^{26,27} The spacers were purchased from commercial suppliers and added to the carboxyl group of the linker using the N-hydroxysuccinimide (NHS) chemistry. The aptamer was purchased with an amino linker and conjugated to the tail-spacer using the NHS chemistry. The aptamer-amphiphile product was purified by reverse phase high performance liquid chromatography (HPLC), and molecular weight was verified by liquid chromatograph–mass spectrometry (LC-MS). All aptamer and aptamer-amphiphile concentrations were measured by absorbance at 260 nm.

Radioactive Competition Binding Assay. Free aptamer was labeled with γ -³²P adenosine triphosphate (ATP). A constant concentration of the labeled free aptamer was mixed with varying concentrations of an unlabeled competitor aptamer or aptamer-amphiphile and incubated with fractalkine in binding buffer (phosphate buffer saline (PBS; salt concentrations provided in Supporting Information) with 50 μ g/mL bovine serum albumin (BSA) and 0.1 μ g/mL of poly(dA:dT), pH = 7.4). Bound aptamer was collected by filtering the solution through a nitrocellulose membrane and the radioactive intensity quantified using a phosphor screen. The IC₅₀ was calculated by fitting the radioactive data to the binding curve equations.

Measurement of Critical Micelle Concentration. The critical micelle concentration (CMC) was found by measuring the increase in fluorescence of Nile red dye with increasing amphiphile concentration.^{28,29} The CMC was the concentration the fluorescence deviated from background levels.

Circular Dichroism Spectroscopy. The aptamer and aptamer-amphiphile were precipitated in ethanol and dissolved to $2.5 \mu\text{M}$ in the appropriate buffer. The sample was heated to 95°C and rapidly cooled to room temperature prior to taking the CD spectrum.

For the melting curves, the aptamer was dissolved in PBS buffer and sealed into a quartz cuvette. The sample was heated at 95 °C for 10 min followed by cooling to 25 °C and heating to 95 °C at 0.25 °C/min. The CD adsorption was measured every 1 °C at 265 and 285 nm.

Cryogenic Transmission Electron Microscopy. The aptamer-amphiphile samples were deposited onto carbon copper grids and vitrified in liquid ethane. The vitrified samples were then imaged on a transition electron microscope.

BESUITS AND DISCUSSION

Radioactive Competition Binding Assay. To create the aptamer-amphiphile the aptamer headgroup must be conjugated to a hydrophobic tail either directly or via a spacer. We

first evaluated the effect of conjugating a hydrophobic tail directly to the aptamer (no spacer was used; NoSPR) on its binding affinity for fractalkine. The C₁₆ dialkyl tail was conjugated at either the 3' or 5' end of the aptamer, and the amphiphile's binding affinity for fractalkine was measured by a radioactive competition binding assay. In this assay, a varying concentration of an unlabeled competitor molecule, either aptamer or aptamer-amphiphile, was added to a constant concentration of free ³²P radiolabeled FKN-S2 aptamer. At high concentrations the unlabeled competitor outcompetes the radiolabeled FKN-S2 aptamer for fractalkine binding sites reducing the measured radioactivity; at low competitor concentrations, the radiolabeled FKN-S2 aptamer primarily binds to fractalkine increasing the measured radioactivity. The IC₅₀ is defined as the concentration at which both FKN-S2 and the competitor bind equally and quantifies the relative affinity between the FKN-S2 aptamer and the competitor molecule.

The IC₅₀ binding curves for the 3'-NoSPR-FKN-S2 (NoSPR tail conjugated to the 3' end of the aptamer) and 5'-NoSPR-FKN-S2 (NoSPR tail conjugated to the 5' end of the aptamer) amphiphiles are shown in Figure 2, and their IC₅₀ values are

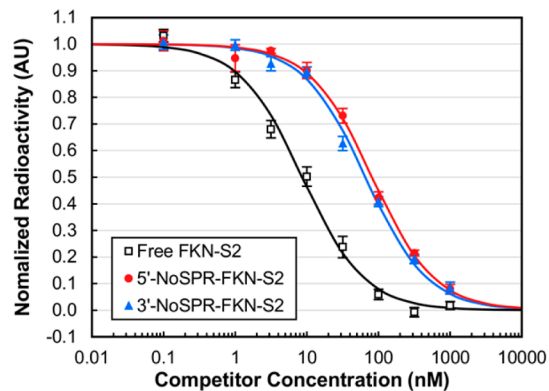


Figure 2. IC₅₀ competition binding curves of the free FKN-S2 aptamer and FKN-S2 aptamer-amphiphiles where the tail was conjugated either at the 3' or 5' end of the aptamer in the absence of any spacer (NoSPR). The data were normalized to the signal at zero competitor concentration. The data show the mean \pm standard error of the mean (SEM) of at least six independent experiments ($n \geq 6$).

given in Table 1. The binding curve of the free FKN-S2 aptamer is shown in black for comparison. Amphiphiles with an IC₅₀ greater than that of the free FKN-S2 aptamer have lower affinity for fractalkine than the free aptamer and vice versa.

Addition of the tail significantly reduced the affinity for fractalkine, and the affinity reduction was orientation specific as shown in Table 1. The 3'-NoSPR-FKN-S2 amphiphile (IC₅₀ of 65.7 \pm 3.5 nM) had a higher affinity than the 5'-NoSPR-FKN-S2 amphiphile (IC₅₀ of 81.6 \pm 6.6 nM) ($p < 0.05$), but both orientations had lower affinity than the free FKN-S2 aptamer (IC₅₀ of 8.6 \pm 0.3 nM). Future aptamer-amphiphiles were synthesized by conjugating the tails and spacers at the 3' end of the aptamer since this aptamer orientation resulted in higher binding affinity-amphiphiles.

Next, the effect of different spacers on the binding affinity of the aptamer-amphiphiles for fractalkine was tested. The amphiphiles were synthesized with either PEG, alkyl (poly-carbon), or oligo-thymine (oligo-T) spacers. Each spacer has different characteristics, and they were chosen to investigate mainly the effect of varying length and hydrophobicity/

Table 1. IC₅₀ Values of the FKN-S2 Aptamer and Aptamer-Amphiphiles^a

sample	IC ₅₀ \pm SEM (nM)
FKN-S2 aptamer	8.6 \pm 0.3
3'-NoSPR-FKN-S2 amphiphile	65.7 \pm 3.5
5'-NoSPR-FKN-S2 amphiphile	81.6 \pm 6.6
3'-PEG ₄ -FKN-S2 amphiphile	68.6 \pm 7.1
3'-PEG ₈ -FKN-S2 amphiphile	47.5 \pm 6.1
3'-PEG ₂₄ -FKN-S2 amphiphile	49.6 \pm 6.1
3'-C ₁₂ -FKN-S2 amphiphile	75.6 \pm 5.6
3'-C ₂₄ -FKN-S2 amphiphile	73.5 \pm 5.6
3'-T ₅ -FKN-S2 amphiphile	37.6 \pm 0.6
3'-T ₁₀ -FKN-S2 amphiphile	21.8 \pm 2.0
5'-T ₁₀ -FKN-S2 amphiphile	55.1 \pm 4.9
3'-A ₁₀ -FKN-S2 amphiphile	24.8 \pm 2.0
3'-T ₅ -FKN-S2 aptamer	3.4 \pm 0.6
3'-T ₁₀ -FKN-S2 aptamer	3.6 \pm 0.9

^aThe affinities of the amphiphiles for fractalkine were measured by competitive binding assays. The lower the IC₅₀ value, the higher the binding affinity of that molecule for fractalkine. IC₅₀ values are reported as the mean \pm SEM ($n = 3-9$). *P*-values from the Student's *t*-test analysis of the IC₅₀ data can be found in Table S1, Supporting Information.

hydrophilicity of the spacer. The PEG spacer is hydrophilic and flexible, the poly-C spacer is hydrophobic, and the oligo-T spacer is negatively charged, flexible, and hydrophilic. The PEG₈ (8 PEG repeats), C₂₄ (24 carbons long), and T₁₀ (10 thymine nucleic acids) spacers have roughly identical lengths. Likewise, the PEG₄, C₁₂, and T₅ spacers have approximately similar lengths. The binding curves of the 3'-NoSPR, 3'-PEG₈, 3'-C₂₄, and 3'-T₁₀ FKN-S2 amphiphiles are shown in Figure 3A with the IC₅₀ values shown in Table 1 (*p*-values from the Student's *t* test analysis of the IC₅₀ data are given in Table S1, Supporting Information). The 3'-NoSPR and 3'-C₂₄ spacers had similar IC₅₀ values of 65.7 \pm 3.5 nM and 73.5 \pm 5.6 nM respectively ($p > 0.05$). The 3'-PEG₈ amphiphile (IC₅₀ of 47.5 \pm 6.1 nM) showed improved affinity compared to the 3'-NoSPR amphiphile ($p < 0.05$). The best amphiphile was clearly the 3'-T₁₀ (IC₅₀ of 21.8 \pm 2.0 nM; $p < 0.001$ with respect to 3'-NoSPR).

The spacer length had a limited effect on the affinity of some amphiphiles (binding curves are shown in Figure S1, Supporting Information, the IC₅₀ values are given in Table 1, and the *p*-values from the Student's *t* test analysis of the IC₅₀ data are given in Table S1, Supporting Information). There was no difference between the C₁₂ and C₂₄ carbon spacers ($p > 0.05$). The affinity of the amphiphile improved from the 3'-PEG₄ amphiphile, IC₅₀ of 68.6 \pm 7.1 nM, to the 3'-PEG₈ amphiphile, 47.5 \pm 6.1 nM, ($p < 0.05$), but there was no difference between the PEG₈ and the PEG₂₄ amphiphiles, 49.6 \pm 6.1 nM ($p > 0.05$). Longer oligo-T spacers seemed to improve the binding affinity of the amphiphiles for fractalkine. The 3'-T₅ amphiphile had an IC₅₀ of 37.6 \pm 0.6 nM, and the 3'-T₁₀ amphiphile had an IC₅₀ of 21.8 \pm 2.0 nM ($p < 0.001$).

Because the 3'-T₁₀-FKN-S2 amphiphile was significantly better than the other amphiphiles, we tested the oligonucleotide derivatives 3'-T₅, 5'-T₁₀, and 3'-A₁₀-FKN-S2 amphiphiles. The 3'-T₅-FKN-S2 amphiphile tested the effect of the oligonucleotide length, the 5'-T₁₀-FKN-S2 tested the effect of the aptamer orientation, and the 3'-A₁₀-FKN-S2 amphiphile tested the effect of the oligonucleotide spacer composition. The

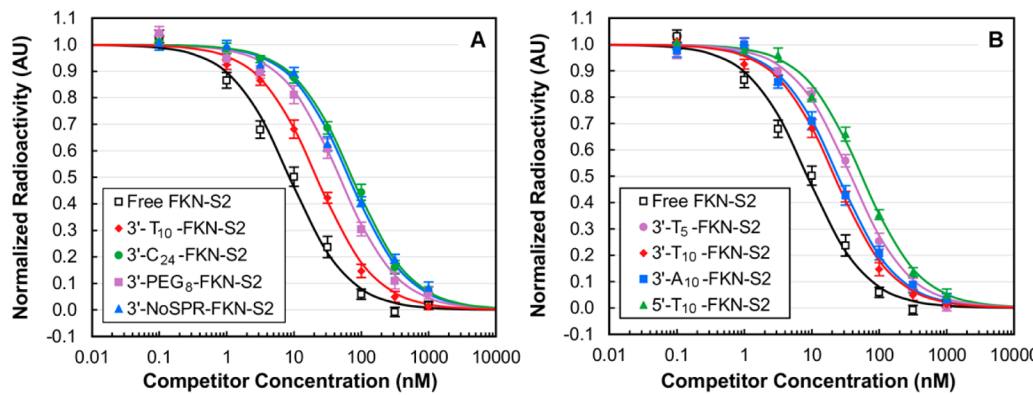


Figure 3. (A) IC₅₀ binding curves of the free FKN-S2 aptamer and 3'-FKN-S2-amphiphiles with T₁₀, PEG₈, NoSPR, and C₂₄ spacers. (B) IC₅₀ binding curves of the free FKN-S2 aptamer and 3'-FKN-S2-amphiphiles with T₁₀, T₅, and A₁₀ spacers and 5'-T₁₀-FKN-S2 amphiphile. The data were normalized to the signal at zero competitor concentration. Data are shown as the mean \pm SEM of at least six independent experiments ($n \geq 6$).

binding curves are shown in Figure 3B. The 5'-T₁₀-FKN-S2 amphiphile (IC₅₀ of 55.1 ± 4.9 nM) performed significantly worse ($p < 0.05$) than the 3'-T₁₀-FKN-S2 amphiphile (IC₅₀ of 21.8 ± 2.0 nM). This is consistent with the preferred 3' aptamer orientation observed when the aptamer was conjugated directly to the tail in the absence of any spacer (3'-NoSPR-FKN-S2 amphiphile shown in Figure 3A). Reducing the oligo-T spacer from 10 to 5 nucleotides significantly reduced the amphiphile affinity. The IC₅₀ value was 21.8 ± 2.0 nM for the 3'-T₁₀-FKN-S2 amphiphile versus 37.6 ± 0.6 nM for 3'-T₅-FKN-S2 ($p < 0.001$). The PEG and oligo-T IC₅₀ data suggest that for short spacers, like PEG₄ and T₅, increasing spacer length increases affinity, but for spacers longer than the PEG₈ no additional gains in affinity were observed. The 3'-A₁₀-FKN-S2 amphiphile, IC₅₀ of 24.8 ± 2.0 nM, performed equally well as the 3'-T₁₀-FKN-S2 amphiphile ($p > 0.05$) suggesting that the nucleotide composition did not affect the affinity.

The oligonucleotide spacer amphiphiles had higher affinities for fractalkine than the PEG or polycarbon spacers, but the reason for this improvement was uncertain. We hypothesized that the improvement in affinity could be the result of the oligonucleotide spacer increasing the affinity of the FKN-S2 free aptamer. To test this, the IC₅₀ values of 3'-T₅-FKN-S2 and 3'-T₁₀-FKN-S2 free aptamers were measured. These aptamers were synthesized as the free aptamer plus the 3' oligonucleotide spacers without the tails. The binding curves are shown in Figure S2, Supporting Information. Interestingly, both the 3'-T₅-FKN-S2 (IC₅₀ of 3.4 ± 0.6 nM) and the 3'-T₁₀-FKN-S2 (IC₅₀ of 3.6 ± 0.9 nM) free aptamers had a higher affinity for fractalkine than the free FKN-S2 aptamer (IC₅₀ of 8.6 ± 0.3 nM; $p < 0.001$ for both 3'-T₅-FKN-S2 and 3'-T₁₀-FKN-S2 with respect to FKN-S2 aptamer). As shown in Table S1 there was no difference between the 3'-T₅-FKN-S2 and 3'-T₁₀-FKN-S2 free aptamers ($p > 0.05$). Because there is no difference in the affinity of the 3'-T₅-FKN-S2 and 3'-T₁₀-FKN-S2 free aptamers, the difference in the affinity of the respective amphiphiles is due to increased spacer lengths between the headgroup and the tail.

Critical Micelle Concentration of Aptamer-Amphiphiles. DNA-amphiphiles have been found to self-assemble into supramolecular structures like micelles. We used the Nile red assay to confirm self-assembly of the FKN-S2 amphiphiles and to measure their CMCs. The Nile red dye fluorescence is much greater in a lyophobic environment than in aqueous solution. At the CMC, when the amphiphiles form micelles, the dye partitions into the hydrophobic micelle core, which results

in an increase in fluorescence. Figure S3, Supporting Information shows a plot of Nile red fluorescence versus aptamer-amphiphile concentration for the 3'-NoSPR-, 3'-PEG₈, 3'-C₂₄, and 3'-T₁₀-FKN-S2 amphiphiles. The fluorescence increases above background levels around 50 nM for each of the amphiphiles. However, due to the lack of sensitivity of the Nile red assay, the CMC of 50 nM should be viewed as an upper limit, which means the different spacer amphiphiles might have differing CMCs, but the assay is not sensitive enough to distinguish. The aptamer-amphiphile CMC is 1–2 orders of magnitude lower than that of peptide-amphiphiles with similar tails. Dialkyl tail peptide-amphiphiles typically have a CMC in the micromolar range.^{30–32} However, similar CMCs in the nanomolar range are seen for other aptamer-amphiphiles.^{12,16}

Circular Dichroism Spectroscopy. The secondary structure of the aptamer may be significantly different in the micelle than when free in solution. Micelles can cause unfavorable base pairing between oligonucleotides, for example, forcing parallel-strand duplex formation between oligo(dA) and oligo(dT).³³ Aptamer-aptamer interactions within a micelle may affect the structure and therefore the binding of the aptamers. Aptamers can adopt a variety of secondary structures including the standard B-form DNA and G-quadruplexes that can be probed using CD. B-form DNA forms from the standard Watson–Crick base pairing between two strands of complementary DNA or within one strand forming stem-loop structures as shown in Figure S4A, Supporting Information. G-quadruplexes are more complex. A G-quadruplex is a tertiary DNA structure composed of stacked G-quartets that form from the general sequence of G_jX_iG_jX_jG_kX_kG_y, where X can be any nucleotide including guanine, y is at least 2, and i, j, k are integers greater than zero.³⁴ A G-quartet is made up of four guanine nucleic acids arranged in a square, planar geometry stabilized by Hoogsteen hydrogen bonds. G-quartets stack due to π bond stacking forming the helical G-quadruplex structure.³⁵ While G-quadruplexes can form in pure water,³⁶ small cations, in particular, K⁺ and to a lesser extent Na⁺, stabilize the formation by fitting inside and between the G-quartets coordinating with the oxygen of guanine.³⁷ G-quadruplexes can be either parallel or antiparallel depending on strand orientation as shown in Figure S4B,C, Supporting Information.³⁵ The G-quadruplex can be either intramolecular (unimolecular) composed of a single aptamer, or intermolec-

ular composed of two (bimolecular) or four (tetramolecular) strands.³⁸

CD spectroscopy was used to probe the secondary structure of the free FKN-S2 aptamer and FKN-S2 amphiphiles. The CD spectra for the free FKN-S2 aptamer were measured in pure water, 20 mM KCl, and PBS buffer (Figure 4A). The water

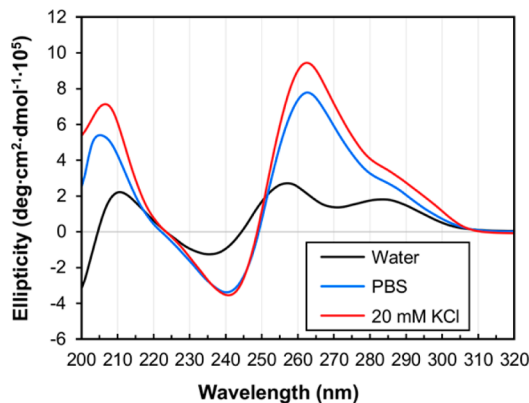


Figure 4. CD spectra of $2.5 \mu\text{M}$ free FKN-S2 aptamer in water, 20 mM KCl, and PBS. The data show the mean of four independent experiments ($n = 4$).

spectrum of FKN-S2 had positive peaks at 285, 258, and 211 nm and a negative peak around 235 nm. The 258 nm peak is characteristic of a parallel G-quadruplex, which typically has a strong positive peak between 258 and 265 nm, while the peak at 285 nm is characteristic of B-form DNA or a stem-loop structure, which typically has a peak between 275 and 285 nm.^{39–41} The CD spectra in 20 mM KCl and PBS show a significant shift. The addition of the salts greatly strengthened the G-quadruplex peak and shifted it to 263 nm, as the salts increase the CD signal of G-quadruplexes by stabilizing the structure.³⁷ The stem-loop peak at 285 nm turned into a shoulder due to the strengthened G-quadruplex peak, but it is still present. The spectrum in PBS buffer is similar in shape to the KCl spectrum but with slightly less signal strength. This is probably because PBS contains mostly Na^+ which does not strengthen the G-quadruplex as strongly as K^+ .³⁷ The G-quadruplex and stem-loop peaks in the spectra shown in Figure 4A suggest the presence of both in the aptamer structure. A hypothetical aptamer secondary structure is shown

in Figure S4D, Supporting Information where the first half of the aptamer, which is G rich, forms a G-quadruplex, and the other half forms a stem-loop structure.

Effect of the Tail and Spacer on the Aptamer Secondary Structure. The CD spectra of the aptamer-amphiphiles were taken in DI water and PBS (Figure 5). The 3'-NoSPR-, 3'-PEG₈-, and 3'-C₂₄-FKN-S2 spectra are nearly identical in water as shown in Figure 5A. Positive peaks occur at 285, 257, and 210 nm, and a negative peak occurs at 236 nm. There was no statistically significant difference in the peak intensity of the 3'-NoSPR, 3'-PEG₈, and 3'-C₂₄-FKN-S2 amphiphiles or the peak location ($n \geq 4$, $p > 0.05$) indicating the secondary structure of the aptamer-amphiphile is similar between the different spacers in water. However, the 3'-T₁₀-FKN-S2 amphiphile differs significantly from the other amphiphiles; it has a much stronger stem-loop peak, the peak has shifted to 281 nm, and a weaker G-quadruplex peak at 260 nm.

The CD spectra of the 3'-NoSPR-, 3'-PEG₈-, and 3'-C₂₄-FKN-S2 amphiphiles in water (Figure 5A) were similar in shape to the free FKN-S2 aptamer spectrum in water (Figure 4A) with the positive and negative peaks occurring at the same wavelengths. However, the G-quadruplex peak at 257–258 nm is stronger for the free FKN-S2 aptamer ($2.7 \text{ deg}\cdot\text{cm}^2\cdot\text{dmol}^{-1}\cdot10^{-5}$ versus $\approx 2.0 \text{ deg}\cdot\text{cm}^2\cdot\text{dmol}^{-1}\cdot10^{-5}$ for free FKN-S2 and the amphiphiles respectively; $p < 0.01$) suggesting that in water, the hydrophobic tails may destabilize the G-quadruplex to a certain extent. There was no difference in intensity of the other spectra peaks. Comparing the 3'-T₁₀-FKN-S2 amphiphile (Figure 5A) and the free FKN-S2 aptamer (Figure 4A), the 3'-T₁₀ amphiphile had a more negative minimum at 236 nm, a depressed peak at 260 nm and a more intense peak at 281 nm than the free FKN-S2 aptamer ($p < 0.01$ for all peak intensities compared to the free aptamer). This suggests the 3'-T₁₀ amphiphile may destabilize the G-quadruplex and stabilize the stem-loop.

The spectra of the aptamer-amphiphiles in PBS are shown in Figure 5B. There is no statistical difference between the peaks of the 3'-NoSPR, 3'-PEG₈, and 3'-C₂₄-FKN-S2 amphiphile spectra ($p > 0.05$). The spectra were strongly characteristic of a parallel G-quadruplex with positive peaks at 262 and 206 nm and a negative peak at 241 nm. The 3'-T₁₀-FKN-S2 amphiphile spectrum has similar characteristics but is slightly different from

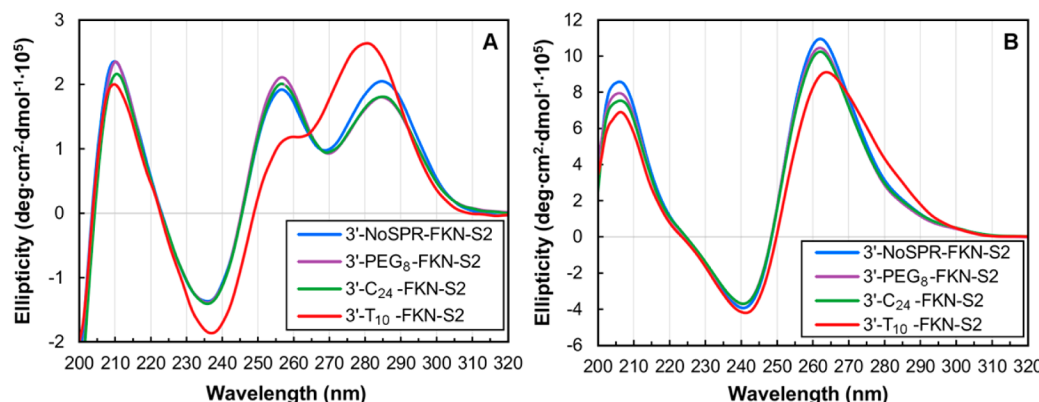


Figure 5. (A) CD spectra of $2.5 \mu\text{M}$ 3'-FKN-S2-amphiphiles in water at 22°C . The data show the mean of at least four independent experiments ($n \geq 4$) with one repetition per experiment. (B) CD spectra of $2.5 \mu\text{M}$ 3'-FKN-S2-amphiphiles in PBS at 22°C . The data show the mean of at least four independent experiments ($n \geq 4$).

the other amphiphiles. The G-quadruplex peak shifts to 264 nm and is less intense.

Comparing the CD spectra of the aptamer-amphiphiles in water and PBS (Figure 5, panels A and B respectively), the PBS buffer shifted the G-quadruplex peak from 257 to 262 nm and increases the intensity 5-fold. This was expected because the K^+ ions of the buffer can stabilize G-quadruplexes. Surprisingly, the stem-loop peak at 285 nm was not present in the aptamer-amphiphile CD spectra in PBS. The 3'-T₁₀-FKN-S2 spectrum broadens slightly at 285 nm, but no peak or shoulder was seen. It is possible the stem-loop is still present in the aptamer-amphiphiles, but the signal is hidden by the large G-quadruplex peak.

The 3'-FKN-S2 amphiphiles (Figure 5B) and the free FKN-S2 aptamer (Figure 4A) CD spectra were similar in PBS except for the absence of the stem-loop shoulder at 285 nm. The peaks occurred at the same wavelengths and the shape was similar. However, the amphiphiles had a much stronger G-quadruplex peak at 262 nm than the free aptamer ($p < 0.01$ when comparing peak intensities) indicating that the addition of the tails stabilized the G-quadruplexes when dissolved in PBS. This was surprising given that the addition of tails seemed to destabilize the G-quadruplex when dissolved in pure water as described earlier. The difference may be due to the ability of PBS to screen the electrostatic repulsion from the negatively charged phosphate backbone. The charge screening of the PBS may promote the G-quadruplex structure that would otherwise be discouraged when the amphiphiles are dissolved in pure water due to electrostatic repulsion.

Melting Curves. Thermal melting studies were performed to further characterize the aptamer and amphiphiles. All melting experiments were done in PBS buffer after we attempted melting experiments in pure water but found the aptamer rapidly degraded at high temperatures, likely through depurination, because of the lack of salts.⁴² The G-quadruplex folding was monitored by CD at 265 nm and the stem-loop at 285 nm. Molar ellipticity was monitored instead of absorbance because the large signal change in CD between unfolded and folded conformations allowed for lower aptamer concentrations. The heating and melting curves of the free aptamer, shown in Figure S5, Supporting Information, overlap indicating reversible melting.

The melting temperature (T_m) was measured as a function of the aptamer concentration to determine the molecularity of the aptamer (Figure S6, Supporting Information). The melting temperature of unimolecular G-quadruplexes are concentration independent, but the melting temperature of bimolecular and tetramolecular quadruplexes increases with increasing concentration.⁴³ The FKN-S2 free aptamer T_m was measured over an aptamer concentration range of 0.25–10 μM . The T_m was constant in the concentration range of 0.25–2.5 μM (Figure S6; $p > 0.05$), but increased at concentrations greater than 2.5 μM . This suggests that at concentrations below 2.5 μM , the free FKN-S2 aptamer forms an intramolecular (unimolecular) G-quadruplex, and at concentrations above 2.5 μM it forms an intermolecular G-quadruplex. A similar transition from intramolecular to intermolecular G-quadruplex has been observed for another aptamer as well.⁴⁴ All CD measurements were taken at 2.5 μM to ensure the aptamer is in unimolecular G-quadruplex.

The thermodynamic stability of the aptamer was assessed by thermal melting experiments. The temperature was decreased at 0.25 °C per min from 95 to 25 °C (cooling curve) and then

increased from 25 to 95 °C (heating curve). No hysteresis was seen at this temperature gradient (Figure S5, Supporting Information) indicating the melting process is reversible and at equilibrium. This allows for calculation of the melting temperature T_m and thermodynamic parameters such as the van't Hoff enthalpy, $\Delta H_{\text{vH}}^\circ$, entropy, ΔS° , and Gibbs free energy, ΔG° . Both $\Delta H_{\text{vH}}^\circ$ and ΔS° are model dependent. The analysis assumes two states, folded and unfolded, are present and that both states are in equilibrium at each temperature. It also assumes the entropy and enthalpy are independent of temperature.⁴³ The thermodynamic parameters for the FKN-S2, 3'-T₅-FKN-S2, and 3'-T₁₀-FKN-S2 free aptamers are shown in Table S2, Supporting Information. There was no difference between the G-quadruplex melting temperatures of the FKN-S2, 3'-T₅-FKN-S2, and 3'-T₁₀-FKN-S2 free aptamers ($p > 0.05$). However, there was a significant difference in the Gibbs free energy. The FKN-S2 aptamer G-quadruplex was more stable (ΔG_{37}° of -13.6 ± 0.10 kJ/mol) than the 3'-T₅-FKN-S2 aptamer (ΔG_{37}° of -12.6 ± 0.14 kJ/mol; $p < 0.01$) and the 3'-T₁₀-FKN-S2 aptamer (ΔG_{37}° of -12.7 ± 0.09 kJ/mol; $p < 0.01$). There was no statistical difference between 3'-T₅ and 3'-T₁₀-FKN-S2 free aptamers; $p > 0.05$. Addition of the oligo-T spacer to the 3' end decreased the stability of the G-quadruplex. Increasing the spacer length from T₅ to T₁₀ did not decrease the stability further.

The trend was similar for the stem-loop DNA peak. The melting temperature did not change ($p > 0.05$), but the stability of the stem-loop increases from a ΔG_{37}° of -21.8 ± 0.5 kJ/mol for the free FKN-S2 to -24.2 ± 0.5 and -24.6 ± 0.7 kJ/mol for the 3'-T₅ and 3'-T₁₀-FKN-S2 free aptamers respectively ($p < 0.05$). There was no significant difference between the 3'-T₅ and 3'-T₁₀-FKN-S2 free aptamers ($p > 0.05$). The oligo-T spacer increases the stability of the stem-loop, but increasing the spacer from T₅ to T₁₀ does not further increase the stability.

The thermodynamics of the aptamer were consistent with the IC₅₀ data (Table 1). The binding curves of the 3'-T₅ and 3'-T₁₀-FKN-S2 free aptamers (Figure S2) were identical and so was the stability of the G-quadruplex and stem-loop secondary structures based on ΔG_{37}° (Table S2). On the basis of the ΔG_{37}° data from Table S2 for the FKN-S2 free aptamer, the G-quadruplex is more stable and the stem-loop less stable compared to the oligo-T FKN-S2 free aptamers. This may suggest that destabilizing the G-quadruplex and stabilizing the stem-loop results in higher affinity of the free aptamer.

The melting curves of the aptamer-amphiphiles were also measured, but they failed to produce usable data (Figure S7, Supporting Information). The melting curves did not plateau at high or low temperatures and the signal intensity did not change much from low temperature to high temperature. Other lipid-oligonucleotide melting curves have shown similar results.^{45,46} The aptamer-amphiphiles retained the G-quadruplex secondary structure even at 95 °C based on CD spectra at various temperatures (Figure S8, Supporting Information). However, no G-quadruplex peak was seen in the FKN-S2 free aptamer spectrum at 95 °C (Figure S9, Supporting Information). Even at 75 °C there is only a small G-quadruplex peak present (Figure S9) which is consistent with the melting curves for the FKN-S2 free aptamer (Figure SSA). It appears that the G-quadruplex formation is stabilized when the amphiphiles are in a micellar structure. From the thermal melting experiments (Figure S6) we know that the FKN-S2 free aptamer forms bimolecular or tetramolecular G-quadruplexes at concentrations above 2.5 μM . In the micelle

headgroup corona layer, the concentration of the aptamer is much higher than in solution because the aptamer is confined at the surface of the micelle. Simple size arguments show that the FKN-S2 aptamer concentration within the micelle is much higher than $2.5 \mu\text{M}$, suggesting the aptamer headgroup forms intermolecular G-quadruplexes within the micelle that may be responsible for the increased melting temperature, and may be more stable than the intramolecular parallel G-quadruplexes seen for the free aptamers.

Cryo-TEM of Aptamer-Amphiphiles. The CMC experiments showed the presence of supramolecular structures. Cryo-TEM images of the FKN-S2 amphiphiles were taken to investigate the shape of the structures (Figure 6). The FKN-S2

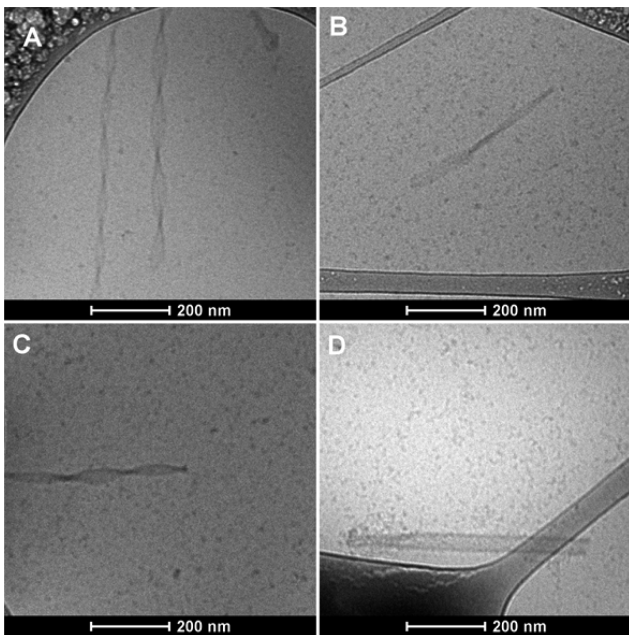


Figure 6. Cryo-TEM images of (A) 3'-NoSPR-FKN-S2 amphiphiles, (B) 3'-PEG₈-FKN-S2 amphiphiles, (C) 3'-C₂₄-FKN-S2 amphiphiles, and (D) 3'-T₁₀-FKN-S2 amphiphiles. All cryo-TEM samples were prepared from stock aptamer-amphiphile solutions at $500 \mu\text{M}$ in DI water.

amphiphiles formed both globular micelles and nanotapes with the majority of the structures being globular micelles. The micelles were found in all the samples and were roughly 10–20 nm in diameter. The nanotape structures were confirmed by tilting the TEM stage at different angles (representative images are shown for the 3'-C₂₄-FKN-S2 amphiphile in Figure S10, Supporting Information). The nanotapes were both flat, Figure 6D, and twisted (Figure 6A–C). Flat and twisted structures were seen in all amphiphiles with similar frequency and the spacer had little effect on the shape of the nanotapes. However, the nanotapes were less prevalent in the 3'-T₁₀-FKN-S2 amphiphile compared to the other spacer amphiphiles.

Even though only micelles were seen in other studies with aptamer-amphiphiles,^{12,16} similar nanotapes were formed by sugar-amphiphiles,⁴⁷ or peptide-amphiphiles with strong hydrogen bonding between the peptide headgroups,^{48,49} and nucleic acid-amphiphiles.^{50,51} The nucleic acid-amphiphiles though that formed nanotape structures all had small headgroups consisting of a single nucleotide and a 12 carbon dialkyl tail.^{50,51}

Work by our group has showed recently that aptamer-amphiphiles can self-assemble into micelles and long nanotapes

that are bilayer structures and can be flat or twisted.¹⁹ The 25 nucleic acid aptamer used in that study (Muc-1 aptamer) had a stem-loop secondary structure (with the potential to form G-quadruplexes as it had guanine nucleotides in its sequence) and was conjugated at its 5' end to C₁₆ dialkyl tails in the absence and presence of different spacers. The aptamer-amphiphiles with NoSPR or PEG spacers self-assembled into micelles, and the assembly process did not significantly alter the secondary structure of the aptamer headgroups as the amphiphiles also had a stem-loop secondary structure. However, in the presence of poly-C spacers the amphiphiles self-assembled into micelles and nanotapes, flat or twisted, with a G-quadruplex intermolecular secondary structure.¹⁹ We hypothesized that the hydrophobic attractions between the poly-C spacers brought the aptamer headgroups together, thus reducing the aptamer headgroup area at the interface and allowing the nanotapes to assemble.

In the current study we found that in water FKN-S2 assumes a stem-loop and G-quadruplex secondary structure as a free aptamer (Figure 4) and as an amphiphile (Figure 5A), independent of the type of spacer used. Furthermore, from the thermal melting studies we postulated that it is possible for the FKN-S2 aptamer headgroup to form intermolecular G-quadruplexes within the self-assembled structures. Therefore, these interactions between adjacent aptamer headgroups could be reducing the headgroup area and favoring the assembly of bilayer nanotapes, similar to the ones observed with the Muc-1 aptamer-amphiphile in the presence of poly-C spacers.

To test this, we synthesized a 40-mer single-stranded DNA (ssDNA) sequence containing no guanine nucleotides (named NoG) thus eliminating the possibility of G-quadruplex formation. The NoG ssDNA had the following sequence, 5'-TTCTATTCTCACATTCATCTATTAAACCACCAATTATT-amino C₆ linker-3'. The sequence was randomly generated from equal probabilities of A, C, and T nucleotides. The 3'-NoSPR-NoG amphiphile and 3'-C₂₄-NoG amphiphile were synthesized and imaged via cryo-TEM (Figure 7). The 3'

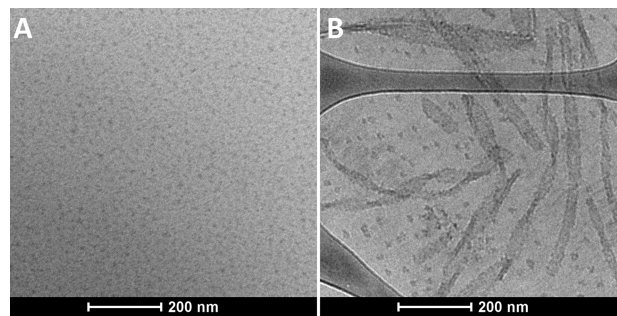


Figure 7. Cryo-TEM images of (A) 3'-NoSPR-NoG amphiphile and (B) 3'-C₂₄-NoG amphiphile.

NoSPR-NoG amphiphile did not form nanotapes, while the 3'-C₂₄-NoG amphiphile formed micelles and flat and twisted nanotapes. This is consistent with the findings of our previous study with the Muc-1 aptamer-amphiphile.¹⁹ Because the NoG ssDNA headgroup does not form intermolecular G-quadruplexes, the 3'-NoSPR-NoG amphiphile does not form nanotapes in the absence of either a G-quadruplex secondary structure or a hydrophobic poly-C spacer that will reduce the aptamer headgroup area by driving the aptamer headgroups in close proximity and allowing the nanotapes to form.

To assess our hypothesis even further, we used a ssDNA sequence, named $(GGGT)_3$, that can form G-quadruplexes. The $(GGGT)_3$ ssDNA with the following sequence, 5'-TTCTATTCTCACATTCATCTATTAAACCGGGTG-GGTGGG-amino C₆ linker-3', was identical to the NoG ssDNA sequence except that 11 nucleotides at the 3' end were replaced with the GGGT repeat where a thymine nucleic acid separated 3 consecutive guanines. The 3' terminal thymine was not included because it was unlikely to participate in G-quadruplex formation. The $(GGGT)_3$ ssDNA sequence cannot form an intramolecular G-quadruplex but is capable of forming intermolecular G-quadruplexes. The CD spectra of the $(GGGT)_3$ free ssDNA, the 3'-NoSPR-(GGGT)₃ amphiphile, and 3'-C₂₄-(GGGT)₃ amphiphile are shown in Figure S11, Supporting Information. The $(GGGT)_3$ free ssDNA does not form G-quadruplexes, but the 3'-NoSPR-(GGGT)₃ and 3'-C₂₄-(GGGT)₃ amphiphiles do. Figure 8 shows cryo-TEM images of

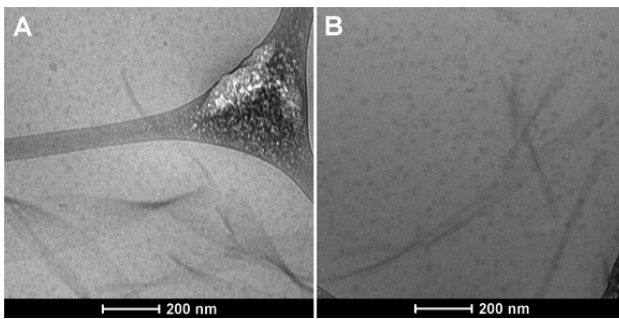


Figure 8. Cryo-TEM images of (A) 3'-NoSPR-(GGGT)₃ amphiphile and (B) 3'-C₂₄-(GGGT)₃ amphiphile.

the amphiphiles. Both the 3'-NoSPR-(GGGT)₃ and 3'-C₂₄-(GGGT)₃ amphiphiles form nanotape structures. In this case, we hypothesize that the intermolecular G-quadruplex formation reduces the headgroup area thus allowing for the assembly of the nanotapes.

Formation and Binding of 3'-T₁₀-FKN-S2 Functionalized Liposomes. Aptamers have potential applications in drug delivery because they are considered to be non-immunogenic and have high affinity and specificity.⁸ Stealth liposomes (liposomes functionalized with PEG) are a well characterized drug delivery vehicle and aptamer-amphiphiles may be used to functionalize stealth liposomes and provide targeting properties to the nanoparticles. Ligand-PEG-lipids have been successfully inserted into the liposome bilayer using a postinsertion technique.⁵² We therefore investigated if the 3'-T₁₀-FKN-S2 aptamer-amphiphile would similarly incorporate into the liposome bilayer using a postinsertion technique. The liposomes were prepared with 5 mol % DPPE-PEG2000 to confer stealth properties to the liposomes. The PEG2000 coating reduces nonspecific interactions with surfaces, proteins, and cells by providing a steric barrier to protein adsorption and cell adhesion.⁵³ The liposomes were functionalized with the 3'-T₁₀-FKN-S2 amphiphile because the IC₅₀ binding experiments (Table 1) showed it had the highest affinity for fractalkine. On average, 79% of the aptamer-amphiphiles incorporated into the liposomes and all of the amphiphiles were on the outside of the liposomes because the liposomes were fully formed before addition of the amphiphiles. The amount of amphiphile functionalization was controlled by changing the amount of amphiphile added to the liposomes during the post insertion

step as shown in Figure S12, Supporting Information. Nonincorporated aptamer-amphiphiles were removed by gel filtration chromatography. To minimize the aptamer-amphiphiles desorbing from the liposomes, the liposomes were stored at 4 °C and used within a week of preparation. Because of these precautions, desorbed aptamer-amphiphiles are not expected to be present at high concentrations during the liposome binding experiments. If present, however, the free aptamer-amphiphiles would act as a blocking agent and reduce liposome binding.

To investigate further the potential of the aptamer functionalized stealth liposomes in targeted drug delivery, the liposomes were targeted to fractalkine expressing cells. The 3'-T₁₀-FKN-S2 functionalized stealth liposomes were loaded with the calcein dye and incubated with MCA-38.FKN mouse colon adenocarcinoma cells transfected to express fractalkine (fractalkine expression levels shown in Figure S13, Supporting Information). The liposomes were incubated for 1 h at 37 °C, and the amount of binding and internalization was quantified using fluorescence as shown in Figure 9.

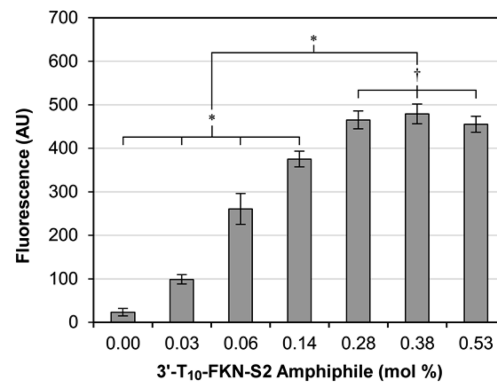


Figure 9. Liposome binding and internalization to fractalkine expressing MCA-38.FKN cells as a function of the concentration of the 3'-T₁₀-FKN-S2 amphiphile used to functionalize the stealth liposomes. Fluorescent liposomes were incubated with the cells for 1 h at 37 °C, and the binding and internalization was quantified by fluorescence. The data show the mean \pm SEM from four independent experiments ($n = 4$). Student's *t* test analysis was used to determine significance, $^{\dagger}p > 0.05$, $^{*}p < 0.05$.

The 3'-T₁₀-FKN-S2 amphiphile functionalized stealth liposomes bound to the cells at all amphiphile concentrations tested. The binding increased with increasing aptamer functionalization. This is expected because liposomes with more aptamers will likely bind with greater avidity due to multiple receptor–ligand interactions. A binding plateaued starting around 0.28 mol % aptamer-amphiphile was observed and may be a result of the liposome-fractalkine binding reaching a saturation point. These experiments showed that the 3'-T₁₀-FKN-S2 amphiphile inserts into stealth liposomes and that the functionalized stealth liposomes bind to fractalkine expressing cells. Further investigation will study the specificity and internalization pathways of the 3'-T₁₀-FKN-S2 functionalized stealth liposomes.

CONCLUSIONS

In this study we synthesized FKN-S2 aptamer-amphiphiles with different spacers and investigated their binding to fractalkine, their secondary structure, and self-assembly. CD spectroscopy suggested the tail and the spacers strengthened the G-quadruplex and destabilized the stem–loop structure of the

FKN-S2 aptamer in PBS, while quite the opposite phenomenon was observed in water. The addition of the tail to the aptamer reduced the affinity of FKN-S2 aptamer for fractalkine for all spacer-tail combinations tested. The 3'-T₁₀-FKN-S2 amphiphile had a much higher binding affinity than the other amphiphiles because of the improved affinity of the free 3'-T₁₀-FKN-S2 aptamer for fractalkine caused by the oligo-T spacer. Melting curve analysis of the free aptamers showed that the oligo-T spacer increased the ΔG°₃₇, thus decreasing stability of the G-quadruplex while increasing the stability of the stem-loop. The CMCs of the FKN-S2 aptamer-amphiphiles were less than 50 nM, and all the FKN-S2 amphiphiles self-assembled into globular micelles and nanotapes, flat or twisted. For the 40-mer ssDNA sequences investigated here, nanotapes were observed in two different cases. In the first case, nanotapes formed from the FKN-S2 and (GGGT)₃ NoSPR amphiphiles because of the strong intermolecular G-quadruplex interactions between the ssDNA headgroups. In the second case, nanotapes did not form in the NoG-NoSPR amphiphiles because the ssDNA headgroup could not form G-quadruplexes. The nanotapes only formed in the presence of a hydrophobic polycarbon spacer. We therefore hypothesized, that in both cases, whether the driving force was the attractive interactions between the ssDNA headgroups or the attractive interactions between the hydrophobic spacers, the aptamer headgroups were brought in close proximity, thus reducing the area per aptamer at the interface allowing the nanotape assemblies to form. Finally, we showed that 3'-T₁₀-FKN-S2 aptamer-amphiphile will post insert into stealth liposomes and that the liposomes were able to bind to fractalkine expressing cells. Further research into the properties of ssDNA amphiphiles could lead to tunable self-assembled aptamer-amphiphiles with molecular recognition properties which can be used for bottom up assembly, targeted drug delivery, and sensors.

■ ASSOCIATED CONTENT

Supporting Information

Detailed experimental materials and methods. Binding curves of PEG, alkyl, and oligonucleotide spacer amphiphiles and aptamer. Student's *t* test *p*-values between IC₅₀ values of the FKN-S2 aptamer and aptamer-amphiphiles. CMCs of the FKN-S2 amphiphiles. Structures of a stem-loop, intramolecular parallel, and intramolecular antiparallel G-quadruplex. Thermal melting curves of the FKN-S2 aptamer and aptamer-amphiphiles. Melting temperature and thermodynamic parameters of the FKN-S2, 3'-T₁₀-, and 3'-T₅- aptamers. Melting temperature of the FKN-S2 free aptamer as a function of aptamer concentration. CD spectra of the FKN-S2 aptamer and aptamer-amphiphiles at different temperatures. Cryo-TEM of a nanotape at 30°, 0°, and -45° stage tilt. CD of the (GGGT)₃ amphiphiles. Post insertion curve of the 3'-T₁₀-FKN-S2 liposome functionalization. Fractalkine expression of the MCA-38.FKN cells. This material is available free of charge via the Internet at <http://pubs.acs.org>.

■ AUTHOR INFORMATION

Corresponding Author

*Phone: (612) 626-1185. Fax: (612) 626-7246. E-mail: kokkoli@umn.edu.

Notes

The authors declare no competing financial interest.

■ ACKNOWLEDGMENTS

The authors thank Prof. Timothy Walseth for his technical support and useful discussions of the IC₅₀ binding assays. This work was supported by the CAREER award NSF/CBET-0846274.

■ REFERENCES

- (1) Laurino, J. P.; Shi, Q.; Ge, J. Monoclonal antibodies, antigens and molecular diagnostics: a practical overview. *Ann. Clin. Lab. Sci.* **1999**, 29 (3), 158–166.
- (2) Ruigrok, V. J. B.; Levisson, M.; Eppink, M. H. M.; Smidt, H.; van der Oost, J. Alternative affinity tools: more attractive than antibodies? *Biochem. J.* **2011**, 436 (1), 1–13.
- (3) Iliuk, A. B.; Hu, L.; Tao, W. A. Aptamer in bioanalytical applications. *Anal. Chem.* **2011**, 83 (12), 4440–4452.
- (4) Cho, E. J.; Lee, J.-W.; Ellington, A. D. Applications of aptamers as sensors. *Annu. Rev. Anal. Chem.* **2009**, 2, 241–264.
- (5) Song, K.-M.; Lee, S.; Ban, C. Aptamers and their biological applications. *Sensors* **2012**, 12 (1), 612–631.
- (6) Walter, J.-G.; Stahl, F.; Scheper, T. Aptamers as affinity ligands for downstream processing. *Eng. Life Sci.* **2012**, 12 (5), 496–506.
- (7) Cerchia, L.; de Franciscis, V. Targeting cancer cells with nucleic acid aptamers. *Trends Biotechnol.* **2010**, 28 (10), 517–525.
- (8) Pangburn, T. O.; Petersen, M. A.; Waybrant, B.; Adil, M. M.; Kokkoli, E. Peptide-and aptamer-functionalized nanovectors for targeted delivery of therapeutics. *J. Biomech. Eng.* **2009**, 131 (7), 074005.
- (9) Tolle, F.; Mayer, G. Dressed for success - applying chemistry to modulate aptamer functionality. *Chem. Sci.* **2013**, 4 (1), 60–67.
- (10) Bouchard, P. R.; Hutabarat, R. M.; Thompson, K. M. Discovery and development of therapeutic aptamers. *Annu. Rev. Pharmacol. Toxicol.* **2010**, 50 (1), 237–257.
- (11) Borisenko, G. G.; Zaitseva, M. A.; Chuvilin, A. N.; Pozmogova, G. E. DNA modification of live cell surface. *Nucleic Acids Res.* **2009**, 37 (4), e28.
- (12) Liu, H.; Zhu, Z.; Kang, H.; Wu, Y.; Sefan, K.; Tan, W. DNA-based micelles: synthesis, micellar properties and size-dependent cell permeability. *Chem.—Eur. J.* **2010**, 16 (12), 3791–3797.
- (13) Cao, Z.; Tong, R.; Mishra, A.; Xu, W.; Wong, G. C. L.; Cheng, J.; Lu, Y. Reversible cell-specific drug delivery with aptamer-functionalized liposomes. *Angew. Chem., Int. Ed.* **2009**, 48 (35), 6494–6498.
- (14) Lao, Y.-H.; Peck, K.; Chen, L.-C. Enhancement of aptamer microarray sensitivity through spacer optimization and avidity effect. *Anal. Chem.* **2009**, 81 (5), 1747–1754.
- (15) Kokkoli, E.; Mardilovich, A.; Wedekind, A.; Rexeisen, E. L.; Garg, A.; Craig, J. A. Self-assembly and applications of biomimetic and bioactive peptide-amphiphiles. *Soft Matter* **2006**, 2 (12), 1015–1024.
- (16) Wu, Y.; Sefah, K.; Liu, H.; Wang, R.; Tan, W. DNA aptamer-micelle as an efficient detection/delivery vehicle toward cancer cells. *Proc. Natl. Acad. Sci. U.S.A.* **2010**, 107 (1), 5–10.
- (17) Tan, W.; Wang, H.; Chen, Y.; Zhang, X.; Zhu, H.; Yang, C.; Yang, R.; Liu, C. Molecular aptamers for drug delivery. *Trends Biotechnol.* **2011**, 29 (12), 634–640.
- (18) Baglioni, P.; Berti, D. Self assembly in micelles combining stacking and H-bonding. *Curr. Opin. Colloid Interface Sci.* **2003**, 8 (1), 55–61.
- (19) Pearce, T. R.; Waybrant, B.; Kokkoli, E. The role of spacers on the self-assembly of DNA aptamer-amphiphiles into micelles and nanotapes. *Chem. Commun.* **2013**, 50 (2), 210–212.
- (20) Waybrant, B.; Pearce, T. R.; Wang, P.; Sreevatsan, S.; Kokkoli, E. Development and characterization of an aptamer binding ligand of fractalkine using domain targeted SELEX. *Chem. Commun.* **2012**, 48 (80), 10043–10045.
- (21) D'Haese, J. G.; Demir, I. E.; Friess, H.; Ceyhan, G. Fractalkine/CX3CR1: why a single chemokine-receptor duo bears a major and unique therapeutic potential. *Expert Opin. Ther. Targets* **2010**, 14 (2), 207–219.

- (22) Jones, B. A.; Beamer, M.; Ahmed, S. Fractalkine/CX3CL1: a potential new target for inflammatory diseases. *Mol. Interv.* **2010**, *10* (5), 263–270.
- (23) Erreni, M.; Solinas, G.; Brescia, P.; Osti, D.; Zunino, F.; Colombo, P.; Destro, A.; Roncalli, M.; Mantovani, A.; Draghi, R.; Levi, D.; Rodriguez y Baena, R.; Gaetani, P.; Pelicci, G.; Allavena, P. Human glioblastoma tumours and neural cancer stem cells express the chemokine CX3CL1 and its receptor CX3CR1. *Eur. J. Cancer* **2010**, *46* (18), 3383–3392.
- (24) Gaudin, F.; Nasreddine, S.; Donnadieu, A.-C.; Emilie, D.; Combadière, C.; Prévot, S.; Machelon, V.; Balabanian, K. Identification of the chemokine CX3CL1 as a new regulator of malignant cell proliferation in epithelial ovarian cancer. *PLoS One* **2011**, *6* (7), e21546.
- (25) Hyakudomi, M.; Matsubara, T.; Hyakudomi, R.; Yamamoto, T.; Kinugasa, S.; Yamanoi, A.; Maruyama, R.; Tanaka, T. Increased Expression of Fractalkine is Correlated with a Better Prognosis and an Increased Number of Both CD8+ T Cells and Natural Killer Cells in Gastric Adenocarcinoma. *Ann. Surg. Oncol.* **2008**, *15* (6), 1775–1782.
- (26) Mardilovich, A.; Kokkoli, E. Biomimetic peptide-amphiphiles for functional biomaterials: the role of GRGDSP and PHSRN. *Biomacromolecules* **2004**, *5*, 950–957.
- (27) Craig, J. A.; Rexeisen, E. L.; Mardilovich, A.; Shroff, K.; Kokkoli, E. Effect of linker and spacer on the design of a fibronectin-mimetic peptide evaluated via cell studies and AFM adhesion forces. *Langmuir* **2008**, *24* (18), 10282–10292.
- (28) Rexeisen, E. L.; Fan, W.; Pangburn, T. O.; Taribagil, R. R.; Bates, F. S.; Lodge, T. P.; Tsapatsis, M.; Kokkoli, E. Self-assembly of fibronectin mimetic peptide-amphiphile nanofibers. *Langmuir* **2010**, *26* (3), 1953–1959.
- (29) Lau, C.; Bitton, R.; Bianco-Peled, H.; Schultz, D. G.; Cookson, D. J.; Grosser, S. T.; Schneider, J. W. Morphological characterization of self-assembled peptide nucleic acid amphiphiles. *J. Phys. Chem. B* **2006**, *110* (18), 9027–9033.
- (30) Tu, R. S.; Marullo, R.; Pynn, R.; Bitton, R.; Bianco-Peled, H.; Tirrell, M. V. Cooperative DNA binding and assembly by a bZip peptide-amphiphile. *Soft Matter* **2010**, *6* (5), 1035–1044.
- (31) Black, M.; Trent, A.; Kostenko, Y.; Lee, J. S.; Olive, C.; Tirrell, M. Self-assembled peptide amphiphile micelles containing a cytotoxic T-cell epitope promote a protective immune response *in vivo*. *Adv. Mater.* **2012**, *24* (28), 3845–3849.
- (32) Lim, Y.-b.; Lee, E.; Lee, M. Controlled bioactive nanostructures from self-assembly of peptide building blocks. *Angew. Chem., Int. Ed.* **2007**, *46* (47), 9011–9014.
- (33) Letsinger, R. L.; Chaturvedi, S. K.; Farooqui, F.; Salunkhe, M. Use of hydrophobic substituents in controlling self-assembly of oligonucleotides. *J. Am. Chem. Soc.* **1993**, *115* (16), 7535–7536.
- (34) Williamson, J. R. G-quartet structures in telomeric DNA. *Annu. Rev. Biophys. Biomol. Struct.* **1994**, *23*, 703–730.
- (35) Huppert, J. L. Four-stranded nucleic acids: structure, function and targeting of G-quadruplexes. *Chem. Soc. Rev.* **2008**, *37* (7), 1375–1384.
- (36) Choi, E. W.; Nayak, L. V.; Bates, P. J. Cancer-selective antiproliferative activity is a general property of some G-rich oligodeoxynucleotides. *Nucleic Acids Res.* **2010**, *38* (5), 1623–1635.
- (37) Kankia, B. I.; Marky, L. A. Folding of the thrombin aptamer into a G-quadruplex with Sr²⁺: stability, heat, and hydration. *J. Am. Chem. Soc.* **2001**, *123* (44), 10799–10804.
- (38) Burge, S.; Parkinson, G. N.; Hazel, P.; Todd, A. K.; Neidle, S. Quadruplex DNA: sequence, topology and structure. *Nucleic Acids Res.* **2006**, *34* (19), 5402–5415.
- (39) Kypr, J.; Kejnovská, I.; Renčík, D.; Vorlíčková, M. Circular dichroism and conformational polymorphism of DNA. *Nucleic Acids Res.* **2009**, *37* (6), 1713–1725.
- (40) Karsisiotis, A. I.; Hessari, N. M. a.; Novellino, E.; Spada, G. P.; Randazzo, A.; Webba da Silva, M. Topological characterization of nucleic acid G-quadruplexes by UV absorption and circular dichroism. *Angew. Chem.* **2011**, *123* (45), 10833–10836.
- (41) Gray, D. M.; Wen, J.-D.; Gray, C. W.; Repges, R.; Repges, C.; Raabe, G.; Fleischhauer, J. Measured and calculated CD spectra of G-quartets stacked with the same or opposite polarities. *Chirality* **2008**, *20* (3–4), 431–440.
- (42) Marguet, E.; Forterre, P. Protection of DNA by salts against thermodegradation at temperatures typical for hyperthermophiles. *Extremophiles* **1998**, *2* (2), 115–122.
- (43) Mergny, J.-L.; Lacroix, L. Analysis of thermal melting curves. *Oligonucleotides* **2003**, *13* (6), 515–537.
- (44) Trajkovski, M.; Webba da Silva, M.; Plavec, J. Unique structural features of interconverting monomeric and dimeric G-quadruplexes adopted by a sequence from the intron of the N-myc gene. *J. Am. Chem. Soc.* **2012**, *134* (9), 4132–4141.
- (45) Shea, R. G.; Marsters, J. C.; Bischofberger, N. Synthesis, hybridization properties and antiviral activity of lipid-oligodeoxynucleotide conjugates. *Nucleic Acids Res.* **1990**, *18* (13), 3777–3783.
- (46) Gosse, C.; Boutorine, A.; Aujard, I.; Chami, M.; Kononov, A.; Cogné-Laage, E.; Allemand, J. F.; Li, J.; Jullien, L. Micelles of lipid-oligonucleotide conjugates: implications for membrane anchoring and base pairing. *J. Phys. Chem. B* **2004**, *108* (20), 6485–6497.
- (47) Jung, J. H.; Do, Y.; Lee, Y.-A.; Shimizu, T. Self-assembling structures of long-chain sugar-based amphiphiles influenced by the introduction of double bonds. *Chem.—Eur. J.* **2005**, *11* (19), 5538–5544.
- (48) Missirlis, D.; Chworus, A.; Fu, C. J.; Khant, H. A.; Krogstad, D. V.; Tirrell, M. Effect of the peptide secondary structure on the peptide amphiphile supramolecular structure and interactions. *Langmuir* **2011**, *27* (10), 6163–6170.
- (49) Ziserman, L.; Lee, H.-Y.; Raghavan, S. R.; Mor, A.; Danino, D. Unraveling the mechanism of nanotube formation by chiral self-assembly of amphiphiles. *J. Am. Chem. Soc.* **2011**, *133* (8), 2511–2517.
- (50) Shimizu, T.; Iwaura, R.; Masuda, M.; Hanada, T.; Yase, K. Internucleobase-interaction-directed self-assembly of nanofibers from homo- and heteroditopic 1,ω-nucleobase bolaamphiphiles. *J. Am. Chem. Soc.* **2001**, *123* (25), 5947–5955.
- (51) Baldelli Bombelli, F.; Berti, D.; Keiderling, U.; Baglioni, P. Giant polymerlike micelles formed by nucleoside-functionalized lipids. *J. Phys. Chem. B* **2002**, *106* (44), 11613–11621.
- (52) Ishida, T.; Iden, D. L.; Allen, T. M. A combinatorial approach to producing sterically stabilized (Stealth) immunoliposomal drugs. *FEBS Lett.* **1999**, *460* (1), 129–133.
- (53) Garg, A.; Tisdale, A. W.; Haidari, E.; Kokkoli, E. Targeting colon cancer cells using PEGylated liposomes modified with a fibronectin-mimetic peptide. *Int. J. Pharm.* **2009**, *366* (1–2), 201–210.